Constructing a warhead of PROTAC with aptamer for tumor-selective degradation of nucleolin

Lin Zhang[1, #], Ling Li[1, #], Xia Wang[1, #], Jing Dai[1], Lingli Zhou[1], Yibin Zhang[1], Tiantian Xie[1], Hui Zhang[1], Tianhuan Peng[1], Xing Sun[1], Hui Li[1], Jing Liu[2], Wencan Wu[3], Mao Ye[1, *], Weihong Tan[1,4 *]

[1]Molecular Science and Biomedicine Laboratory (MBL), State Key Laboratory of Chemo/Biosensing and Chemometrics, College of Biology, College of Chemistry and Chemical Engineering, Aptamer Engineering Center of Hunan Province, Hunan University, Changsha, Hunan 410082, China

[2]Molecular Biology Research Center and Center for Medical Genetics, School of Life Sciences, Central South University, Changsha, Hunan 410078, China

[3]The Eye Hospital of Wenzhou Medical University, Wenzhou, Zhejiang 325027, China

[4]The Cancer Hospital of the University of Chinese Academy of Sciences (Zhejiang Cancer Hospital), Institute of Basic Medicine and Cancer (IBMC), Chinese Academy of Sciences, Hangzhou, Zhejiang 310022, China

#These authors contributed equally to this work.

*To whom correspondence should be addressed. E-mail: goldleaf@hnu.edu.cn or tan@hnu.edu.cn

Abstract:

PROteolysis TArgeting Chimeras (PROTACs) induce targeted protein degradation by hijacking the intracellular ubiquitin proteasome system, thus emerging as a new strategy for drug development. However, although PROTACs are highly efficient for protein degradation, most PROTACs generated lack cell-type selectivity, resulting in potential off-tissue, on-target toxicity. To address this drawback, we herein developed an aptamer-based PROTAC ZL216 using aptamer AS1411 as a targeting ligand for nucleolin, and it showed both excellent serum stability and water solubility. Based on the differential expression of nucleolin on the cell surface, ZL216 can specifically bind to and internalize into breast cancer cells, but not normal breast cells. Furthermore, we revealed that ZL216 promoted the formation of a nucleolin-ZL216-VHL ternary complex in breast cancer cells and potently induced the degradation of nucleolin *in vitro* and *in vivo*, thereby inhibiting the proliferation and migration of breast cancer cells. These studies demonstrated the potential of utilizing aptamers to construct PROTACs to achieve the selective degradation of targeted protein in tumor cells and provided a promising strategy for the development of tumor-selective PROTACs.

Introduction:

PROteolysis Targeting Chimeras (PROTACs) are small molecules with heterobifuntional property, consisting of a ligand for binding to a protein of interest (POI) and the other for recruiting an E3 ubiquitin ligase via a linker connection. Such molecules can tether an E3 ligase to POI by forming a ternary complex, thereby triggering proximity-induced ubiquitination and degradation of POI in a catalytic manner. PROTACs have been developed to degrade proteins that play important roles in tumorigenesis and do so with extraordinary efficacy on multiple tumor types, including BRAF mutant V600E for melanoma [1], BET for prostate cancer [2], BCL-X_L for leukemia [3] and Estrogen Receptor (ER) for breast cancer [4]. Until present, at least 15 targeted protein degraders are expected to be carried out in patients at different stages of human clinical trials [5]. However, although PROTACs are highly efficient for protein degradation and, hence, a potential therapeutic strategy for cancer, most PROTACs generated lack tumor selectivity, essentially because the E3 ligases utilized by PROTACs are widely expressed in both normal and tumor tissues. As a result, these PROTACs may produce on-target toxicity if POIs are not tumor-specific. This calls for the development of selective ligands able to restrict the activity of PROTACs to tumor cells, but not normal cells, thus generating tumor-selective PROTACs.

Aptamers are single-stranded DNA or RNA oligonucleotides with a length typically less than 100 nucleotides. Aptamers are generated by an iterative

selection process termed systematic evolution of ligands by exponential enrichment (SELEX) from a randomized oligonucleotide library [6]. Similar to antibodies, aptamers bind to their targets with high specificity and affinity by folding into a unique three-dimensional conformation. Compared to protein antibodies, aptamers hold unique characteristics derived from their oligonucleotide properties, such as low immunogenicity and toxicity, easy chemical synthesis and modification, rapid tissue penetration and excellent stability[7]. With the advent of cell-specific aptamers, aptamers have been widely used as tumor recognition ligands for targeted therapy, detection and diagnostics. For example, CD71 ssDNA aptamer was coupled with doxorubicin to specifically target tumor cells and inhibit their proliferation [8].

AS1411 is a 26-base guanine-rich ssDNA aptamer, which binds to nucleolin with high affinity and specificity. Many studies have indicated that enhanced expression of nucleolin on the cell surface is restricted to tumor cells, but not normal cells, thus conferring a tumor-selective binding behavior to AS1411[9]. Meanwhile, AS1411 can be internalized into tumor cells by nucleolin-dependent macropinocytosis [10] and subsequently exert antiproliferative activity against a wide range of tumor types, including breast cancer [11], glioma [12], renal cell carcinoma [13] and leukemia [14]. Thus, AS1411 potentially acts as both a tumor-targeting element and an anticancer therapeutic agent.

In this study, we report the first proof-of-concept evidence using an

aptamer to obtain a tumor-selective PROTAC. Aptamer AS1411, as a targeting ligand for nucleolin, was conjugated via a connecting linker to a small molecule ligand of E3 ligase VHL, which generated AS1411-based PROTAC ZL216 with excellent serum stability and water solubility. We demonstrated that ZL216 could recruit E3 ligase VHL to nucleolin in breast cancer cells and potently induce the degradation of nucleolin *in vitro* and *in vivo*. As a result, ZL216 inhibits the proliferation and migration of breast cancer cells. Our work demonstrates the potential use of aptamers in generating PROTACs to achieve selective degradation of targeted protein in tumor cells and provides a promising strategy for development of tumor-selective PROTACs.

Results:

Development of aptamer-based PROTAC ZL216 for nucleolin degradation

By analyzing various cancer types found on the TCGA database using TIMER2.0, we found that the gene expression levels of nucleolin in multiple tumor tissues, including breast cancer tissues, were significantly higher than those of normal tissues (Figure S1A). Consistent with this, the result of the CPTAC proteomics database also showed elevated protein levels of nucleolin in breast cancer tissues compared to corresponding normal tissues (Figure S1B). We further confirmed this finding in cell lines by Western blotting, which showed enhanced expression of nucleolin protein in breast cancer cells (MCF-7 and BT474), but not in immortalized breast epithelial cells (MCF-10A) (Figure

S1C). Moreover, a part of nucleolin was distributed at the surface of MCF-7 and BT474 cells, but not the surface of MCF-10A cells (Figure S1D), which is consistent with the notion that the expression of nucleolin on the cell surface is restricted to tumor cells.

AS1411 functions as an ssDNA aptamer that can bind to nucleolin with high affinity and specificity and that it is quickly internalized into cells following binding to nucleolin. Given the critical role of nucleolin in supporting tumorigenesis and metastasis, we hypothesized that an AS1411-PROTAC conjugate could achieve targeted antitumor activity through promoting nucleolin degradation specifically in tumor cells (Figure 1A). To test the possibility, AS1411, as a targeting element for nucleolin, was conjugated via a connecting linker to a VHL E3 ligase-binding ligand AHPC to generate the aptamer-based nucleolin degrader ZL216 (Figure 1B), whereas an ssDNA sequence, which has no affinity for nucleolin, was linked to AHPC as a negative control (Figure S2A). In addition, the synthesis and characterization of Cy5-labeled control and ZL216 were shown in Figure S2B and S2C. To identify the stability of ZL216 in serum, ZL216 and AS1411 were incubated with human serum. We found that ZL216 holds an excellent serum stability, similar to that of AS1411, with a half-life of more than 72 hours (Figure 1C). Meanwhile, the water solubility of ZL216 was significantly enhanced compared to that of free VHL E3 ligase-binding ligand AHPC through conjugation with aptamer AS1411 (Figure S3).

Selective binding ability of ZL216

Previous studies have shown that AS1411 can specifically bind to breast cancer cells through recognizing cell-surface nucleolin. To assess whether ZL216 still retains the binding specificity to breast cancer cells, cells were incubated with Cy5-labeled AS1411, ZL216 and Controls, respectively. As shown in Figure 2A, 2B and 2C, a significant fluorescence peak shift was observed from MCF-7 and BT474, but not MCF-10A cells, indicating that ZL216 held its binding specificity to breast cancer cells in a manner similar to that of AS1411. Meanwhile, the selective binding ability of ZL216 was further confirmed by confocal imaging (Figure 2D, 2E and 2F). To identify whether ZL216 has the same binding sites as AS1411, a competitive binding assay was performed by flow cytometry. Different concentrations of unlabeled AS1411 were incubated with Cy5-labeled ZL216. Intriguingly, ZL216 gradually lost its binding to MCF-7 and BT474 cells as the concentration of AS1411 increased, whereas the control showed no effect from the binding between ZL216 and MCF-7 or BT474 cells, implying that the same binding sites were shared by ZL216 and AS1411(Figure 2G and 2H). Furthermore, the binding affinity assay showed that the Kd of ZL216 for MCF-7 and BT474 cells was 11.42 ± 4.924 nM and 21.54 ± 7.629nM, while the Kd of AS1411 on MCF-7 and BT474 cells was 17.14 ± 16.19nM and 47.36 ± 13.1nM, respectively (Figure 2I and 2J), suggesting that ZL216 has stronger binding ability than AS1411 alone. We

speculate that the mechanism underlying this enhanced binding ability might be associated with the role of the conjugate in stabilizing the dynamic binding of AS1411.

ZL216 specifically attenuates nucleolin of breast cancer cells *in vitro and in vivo*

Internalization into cells directly determines whether aptamer-based PROTACs can hijack the intracellular ubiquitin-proteasome system. To investigate the internalization property of ZL216, intracellular fluorescence signals were detected by flow cytometry after eliminating the fluorescence signals on the cell surface by trypsin or proteinase K. As shown in Figure S4A and S4B, the removal of the fluorescence signals on the cell surface reduced, rather than eliminated, the fluorescence signals from target cells, indicating that a fraction of ZL216 could be internalized into target cells. Next, we evaluated ZL216 for its ability to regulate nucleolin levels. After cells were treated with different concentrations of ZL216, nucleolin abundance was analyzed by Western blotting. We found that ZL216 could effectively downregulate nucleolin levels in MCF-7 and BT474 cells (Figure 3B and 3C). At the 5-h time point, the half-maximal inhibition concentration (DC_{50}) and maximum inhibition (D_{max}) of MCF-7 cells were 8.3 nM and 82%, while those of BT474 cells were 17.8 nM and 87%, respectively. In contrast, ZL216 failed to reduce nucleolin level in MCF-10A cells (Figure 3A). The time dependency of ZL216 on nucleolin showed that maximal reduction of nucleolin was achieved at 48 h for MCF-7

cells (Figure 3E) and 5 h for BT474 cells (Figure 3F). In addition, both AS1411 and an E3 ligase-binding ligand AHPC had no effect on nucleolin levels (Figure S5A and S5B). Furthermore, to determine whether ZL216 retains its recognition ability and reduces nucleolin levels *in vivo*, we generated MCF-7 and BT474 xenografts in mice and then treated the mice with Cy5-labeled ZL216, AS1411 and control via tail vein injection. As expected, the fluorescence signal was rapidly accumulated at the tumor sites after injecting ZL216 and AS1411, while no significant fluorescence signal was observed at the tumor sites treated with control, indicating that ZL216 held the same ability to target tumor *in vivo* as that achieved by AS1411 (Figure 3G and 3H). Notably, ZL216 could decrease nucleolin levels in xenografts (Figure 3I and 3J). In contrast, neither AS1411 nor AHPC had any effect on nucleolin levels (Figure 3K and 3L). This result highlighted that ZL216 not only possessed an ability to target tumors similar to that of AS1411, but also had the added benefit of reducing nucleolin levels, not otherwise achievable by AS1411.

ZL216 degrades nucleolin in a VHL- and proteasome-dependent manner

To confirm that ZL216 causes the reduction of nucleolin levels through the expected degradation mechanism via proteasome, we first tested the effect of ZL216 on the expression of nucleolin mRNA by real-time PCR. We found that the levels of nucleolin mRNA were not regulated by ZL216, control, AHPC or AS1411 (Figure 4A and 4B), indicating that ZL216 does not affect nucleolin

expression at the transcriptional level. Furthermore, downregulation of nucleolin caused by ZL216 could be abolished by a proteasome inhibitor, MG132, or a cullin neddylation inhibitor, MLN4924 (Figure 4C and 4D), suggesting that ZL216 decreased nucleolin levels through the proteasome degradation pathway. To further identify whether ZL216 degrades nucleolin via VHL, cells were treated with a high concentration of free AHPC to compete for the binding of ZL216 to VHL. The results showed that an excess amount of AHPC could significantly attenuate the effect of ZL216 on nucleolin in MCF-7 and BT474 cells (Figure 4E and 4F), demonstrating that ZL216-mediated regulation of nucleolin protein levels depended on VHL. Since ZL216 downregulated nucleolin protein levels, we questioned whether ZL216 affected the stability of nucleolin. To this end, cells were treated with cycloheximide (CHX) to inhibit protein biosynthesis, followed by analyzing nucleolin protein at indicated time points. We found that ZL216 treatment significantly shortened the half-life of nucleolin protein compared with control treatment (Figure 4G and 4H).

ZL216 induces the formation of nucleolin-ZL216-VHL ternary complex

Nucleolin is not the intracellular natural substrate of the E3 ligase VHL. We hypothesized that ZL216 may mediate the degradation of nucleolin through the formation of a nucleolin-ZL216-VHL ternary complex. To address this, Flag-VHL and Myc-NCL plasmid were transfected into MCF-7 cells, and

coimmunoprecipitation was conducted using anti-Flag or anti-Myc antibody. The results indicated that Myc-nucleolin was present in Flag-VHL immunoprecipitates after cells were treated with ZL216 and vice versa (Figure 5A and 5B). Conversely, treatment with control, which lacks nucleolin binding, failed to detect the expected protein in Flag-VHL or Myc-nucleolin immunoprecipitates. Immunofluorescence staining further revealed that ZL216, but not control treatment, caused the colocalization of nucleolin and VHL (Figure 5C). Because the E3 ligase catalyzes proximity-induced ubiquitination of substrate, we questioned whether the formation of ternary complex induced by ZL216 contributed to nucleolin ubiquitination. To this end, the ubiquitination levels of nucleolin were measured. As expected, ZL216 significantly increased the ubiquitination levels of nucleolin, whereas DMSO and control exhibited no effect on nucleolin ubiquitination (Figure 5D and 5E). Collectively, these results suggest that ZL216 promotes nucleolin ubiquitination by inducing nucleolin-ZL216-VHL ternary complex formation.

To investigate the molecular basis of nucleolin-ZL216-VHL ternary complex formation, molecular docking and dynamics simulation were performed. A total of 100 conformations were extracted and ranked by docking energy value. Since low-energy conformations help reveal detailed intermolecular interaction and stable bonding interface, conformations with the lowest binding energy were chosen to predict the binding spots. The result showed that the binding mode between nucleolin and AS1411 was mainly dependent on hydrophobic

bonds with the binding energy of -123 kcal/mol, whereas the binding between VHL and AHPC appeared to be maintained by the formation of polar hydrogen bonds with docking energy of -7.99 Kcal /mol (Figure 5F). The above results implied that ZL216 could interact with nucleolin and VHL with high binding affinity.

ZL216 inhibits the proliferation and migration of breast cancer cells via VHL binding

To address whether the ZL216-induced degradation of nucleolin affects the proliferation and migration of breast cancer cells, we performed a cell proliferation and migration assay in MCF-10A and MCF-7 cells. The results showed that ZL216 treatment dramatically inhibited the proliferation of MCF-7 cells, but had no effect on MCF-10A cells (Figure 6A and 6B). A wound healing assay demonstrated that ZL216 treatment significantly reduced the migration of MCF-7, but not MCF-10A, cells (Figure 6C and 6D). Consistently, a similar result was observed in transwell assay, and MCF-7, but not MCF-10A, cells in lower layer after ZL216 treatment were notably fewer in number compared to control treatment (Figure 6E and 6F). The selective effect was consistent with the specific degradation of nulceolin induced by ZL216 in breast cancer cells. Interestingly, the effect of ZL216 on MCF-7 cells could be abolished by pretreatment with 1μM AHPC (Figure 6A, 6B, 6C, 6D, 6E and 6F), implying that the anti-proliferation and anti-migration activities of ZL216 were dependent on

VHL binding. Of note, although previous studies showed that AS1411 retained its functional activity against breast cancer, we found that AS1411 treatment failed to show any effect on MCF-7 cells. This might be explained by the lower concentration of AS1411 treatment.

Discussion

PROTACs function as a designed heterobifunctional molecule to induce the degradation of unwanted protein by hijacking the intracellular ubiquitin-proteasome system. Early PROTACs were developed based on bifunctional peptides that recruited E3 ligases to degrade targeted proteins [19, 20]. However, peptide-based PROTACs suffered from low cell permeability and, hence, poor cellular activity, hindering the broad applicability of PROTACs[21]. Subsequently, owing to the identification of small-molecule-based E3 ligase ligands, such as nutlin-3a for MDM2 [22], thalidomide for CRBN [23] and VH032 for VHL [24], a series of small-molecule-based PROTACs were developed, which represents a significant advancement in PROTAC technology. In this study, we further developed the first aptamer-based PROTAC ZL216 through conjugating ssDNA aptamer AS1411 with a small-molecule ligand of VHL. ZL216 promoted the formation of nucleolin-ZL216-VHL ternary complex by using AS1411 as a ligand for binding to nucleolin, which potently induced the degradation of nucleolin *in vitro* and *in vivo*. Currently, few aptamers that specifically bind to E3 ligases are available; therefore, we only utilized the

aptamer as a protein of interest (POI) ligand to construct PROTAC. The development of specific aptamers for E3 ligases will contribute to the generation of heterobifunctional aptamers to achieve the function of PRTOACs.

It is estimated that the human genome encodes more than 600 E3 ligases [25]. However, the number of E3 ligases currently used for PROTAC development is still very small, mainly including VHL, CRBN, MDM2 and cIAP1 [21]. Previous studies show that PROTACs based each of these E3 ligases hold different characteristics, such as specificity, efficacy, or toxicity. For example, despite using the same BCR-ABL ligand as a warhead, the CRBN-based PROTACs destroyed both BCR-ABL and c-ABL, while the VHL-based PRTOACs only had an effect on c-ABL [26]. In this study, we developed a VHL-recruiting PROTAC using aptamer AS1411 as a nucleolin ligand. We demonstrated that the conjugate induced nucleolin degradation via the ubiquitin proteasome pathway in a VHL-dependent manner. Nevertheless, it is worth investigating if AS1411 can be conjugated with other E3 ligases and still degrade nucleolin. PROTACs promote the ubiquitination and degradation of targeted protein by inducing spatial proximity between an E3 ligase and target protein via the formation of a ternary complex. The spatial distance between E3 ligase and targeted protein is critical to the efficacy of PROTACs. Of note, aptamers have a length ranging from approximately 20 to 80 nucleotides. Whether aptamer length affects the formation and stability of ternary complex and the ability of a PROTAC to degrade its target are questions that need further

clarification in the future.

The water solubility of PROTACs is critical to its cell permeability and efficacy. AS1411 is a synthetic 26-base guanine-rich ssDNA oligonucleotide. Previous studies have shown that the water solubility of paclitaxel could be improved by conjugating AS1411 and paclitaxel [27]. The small-molecule E3 ligase ligand APHC exhibited poor water solubility, but consistent with the above results, our AS1411-AHPC conjugate ZL216 showed a significant enhancement in water solubility, implying that a hydrophilic nucleic acid aptamer integrated into PROTACs can improve their water solubility.

AS1411 binds to nucleolin with high affinity and specificity. Many studies have indicated that enhanced expression of nucleolin on the cell surface is restricted to tumor cells, but not normal cells, which confers a tumor-selective binding behavior to AS1411. Our results showed that the aptamer-based PROTAC ZL216 using AS1411 as a targeting element for nucleolin still retained the same tumor-selective property as free AS1411. However, unlike AS1411, ZL216 induced tumor-specific nucleolin degradation *in vitro* and *in vivo* by recruiting E3 ligase VHL. Previous studies have shown that AS1411 exhibited antitumor activity. Unexpectedly, a weak activity was observed for AS1411 in our studies. This phenomenon may be explained in different ways. ZL216 functions as a PROTAC to promote nucleolin degradation, whereas AS1411 does not affect nucleolin levels, but rather regulates the function of nucleolin. In addition, the concentration range we set was based on the activity of ZL216,

which is in nanomolar range. However, AS1411 has been reported to inhibit the growth of cancer cells in micromolar range [28, 29]. This finding is consistent with previous studies that PROTACs generally achieve a desired pharmacological effect at significantly lower concentration owing to its catalytic mode of action [30, 31].

Materials and Methods

Reagents. The following reagents were used in this study: the Von Hippel-Lindau (VHL) E3 ligand (S,R,S)-AHPC-PEG3-azide (AHPC) (Sigma Aldrich), MG132 (Sigma Aldrich), MLN4924 (S7109, Selleck Chemicals), anti-nucleolin antibody (D4C7O, Cell Signaling Technology), anti-β-Tubulin antibodies (9F3, Cell Signaling Technology), anti-mouse IgG Alexa Fluor® 488 Conjugate (4408, Cell Signaling Technology), anti-rabbit IgG Alexa Fluor® 594 Conjugate antibodies (8889, Cell Signaling Technology), anti-VHL antibody (sc-135657, Santa Cruz), anti-Ub (sc- 166553, Santa Cruz), anti-β-Actin antibody (AT0001, Engibody), anti-Flag antibody (20543-1-AP, Proteintech) anti-MYC antibody (M192-3, MBL International), anti-HA antibody (M180-3, Medical & Biological Laborato), Cell Counting Kit-8 (CCK-8) (New Cell & Molecular Biotech), Agarose and Super GelRedTM (S2001, US Everbright®Inc) and Cell Culture flasks (NEST Biotechnology). All DNA sequences were synthesized by Hippobio Technology (Zhejiang, China) and Shenggong Biotechnology (Shanghai, China).

Synthesis of ZL216 and Control. (S, R, S)-AHPC-PEG3-azide was dissolved in DMSO at a concentration of 10 mM. DBCO-AS1411 and DBCO-control sequences were dissolved in ddH2O at a concentration of 100 μM. After that, they were mixed under mechanical stirring at room temperature, and the click reaction between an azide and DBCO was performed overnight. The solution was then purified by HPLC and verified by mass spectrometry. The synthetic methods and identification of Cy5-ZL216 and Cy5-Control were the same as described above.

Cell culture. Human breast cancer cell line BT474 was cultured in RPMI-1640 containing 10% fetal bovine serum (FBS). Human breast cancer cell line MCF-7 was cultured in high-glucose Dulbecco's Modified Eagle's Medium (DMEM) containing 10% fetal bovine serum (FBS). Normal human epithelial mammary cell line MCF-10A was maintained in complete medium purchased from Cellcook Biotech Company. All cells were cultured at 37 °C in an incubator containing 5% CO2.

Flow Cytometry Analysis. The binding abilities of ZL216 and AS1411 were determined by flow cytometry. Cy5-labeled ZL216, AS1411 and Control were incubated with 0.2% EDTA-treated cells (2×10^5) in 200 μL binding buffer (BB; DPBS, 5 mM $MgCl_2$, 4.5 mg/mL glucose, 1 mg/mL BSA, and 0.1 mg/mL yeast

tRNA) at 37℃ for 40 min. Then, cells were washed twice with washing buffer (WB; 5 mM MgCl2 and 4.5 g/L glucose in Dulbec-co's PBS), resuspended in 400 μL DPBS and then subjected to flow cytometric analysis.

To explore the expression of nucleolin on the cell plasma membrane,0.2% EDTA-treated cells were blocked in 5% BSA buffer for 30 min at 4℃ and then incubated with anti-nucleolin primary antibody (1:400 in 1% BSA buffer) for 1 h at 4℃. Cells were washed 3x in DPBS and incubated with Alexa Fluor 647-conjugated goat anti-rabbit IgG (diluted 1:200 in 1% BSA buffer) for 30 min at room temperature. After that, cells were washed 3x in DPBS and then subjected to analysis by flow cytometry.

Live cell confocal microscopy. After 2×10^5 cells were seeded in a 35-mm glass bottom dish for 24 h, we incubated cells with Cy5-labeled ZL216 or Control in 200 μL BB at 37℃ for 2 h. After washing cells three times with WB, confocal laser scanning microscopy (Carl Zeiss) was used to detect fluorescent signals.

In Vitro Stability assay. 2 μM Cy5-labeled AS1411 and ZL216 were incubated in human serum at 37 ℃ for 0,2, 4, 6, 8, 10, 12, 24, 48, 72, and 96 h. Then, aptamers were visualized on a 0.5% agarose gel (containing 1% SDS); the band density was assayed by molecular imaging (Bio-Rad).

Real-Time PCR. MCF-7 cells were incubated with 25 nM ZL216, Control, AHPC,

AS1411 or DMSO for 5 h and the total RNA extracted using Eastep (Promega catalog no. LS1040). 1 μg of purified RNA was reverse-transcribed in a 20 μL reaction using a FastQuant RT Super Mix Kit (TIANGEN, catalog no. KR106-02). Real-Time PCR was then performed by using Maxima SYBR Green/ROX kit (ThermoFisher Scientific) on an Applied Biosystem ABI 7500 Real-Time PCR system with the following primer sequences:

NCL-F GCACCTGGAAAACGAAAGAAGG;

NCL-R GAAAGCCGTAGTCGGTTCTGT;

GAPDH-F ATGTTCGTCATGGGTGTGAA;

GAPDH-R TGTGGTCATGAGTCCTTCCA.

BT474 cells were incubated with 50 nM ZL216, Control, AHPC, AS1411 or DMSO for 5h, followed by performing the mRNA levels of NCL using the same method as described above.

Western blot analysis. After 2×10^5 cells were seeded in a 12-well plate for 24 h, we treated cells with ZL216/Control/AS1411/AHPC at certain times. Then cells were lysed in RIPA buffer (catalog no. P0013B, Beyotime) supplemented with protease inhibitors (EDTA-free Protease Inhibitor Tablets, catalog no. 88266, Pierce). Lysates were centrifuged at 15,000 rpm for 15 min, and the supernatants were used for Western blot analysis.

Cycloheximide (CHX) assay. MCF-7 or BT474 cells were pretreated with

cycloheximide (100 μg·mL−1) for 1 h, prior to adding either vehicle (DMSO) or ZL216 (25 nM or 50 nM). At the indicated time points, cells were lysed. The protein levels were assessed using Western blot analysis

Proteasome-dependency experiment. 2×10^5 MCF-7 or BT474 cells were cultured in a 12-well plate for 24 h and then incubated in 20 μM MG132 (dissolved in DMSO) or equal volume of DMSO for 1 h. Cells were then treated with 25 nM or 50 nM ZL216 for another 5 h, harvested, followed by analysis of lysates by Western blot assay.

Co-Immunoprecipitation (Co-IP). MCF-7 cells were transfected with Myc-NCL and Flag-VHL expression plasmids by using LipoMAXTM Reagent (SUDGEN). After 24 h, cells were treated with 20 μM MG132 for 1 h followed by 25 nM ZL216 or Control and incubated for an additional 5 h. Thereafer, cells were lysed in M-PER (Thermo Fisher Scientific catalog no.78501) supplemented with protease inhibitors (Bimake no. B14011). Cell lysates were centrifuged at 15,000 rpm for 15 min, and supernatants collected. 3 μg of relevant primary antibodies were incubated with the lysate (total proteins) at 4℃ overnight, followed by the addition of 30 μL of magnetic beads conjugated with protein G (Invitrogen, catalog no. 10004D) for 1 h and eluted by co-IP washing buffer. Finally, the pulled down proteins were dissolved in 2×SDS sample buffer, boiled, and subjected to Western blot analysis.

In Vivo Ubiquitylation assay. MCF-7 cells cotransfected, or not, with Myc-NCL, Flag-VHL and HA-ubiquitin plasmid for 24 h, were pretreated with 20 μM MG132 for 1 h before adding 25 nM ZL216 or Control. Cells were lysed, and lysates were then incubated with an anti-NCL or anti-Myc antibody at 4°C overnight followed by protein A/G agarose beads for an additional 1 h at room temperature. The proteins were released from beads by boiling the beads in SDS/PAGE sample buffer. The ubiquitination of NCL or Myc-NCL was detected by Western blot with anti-Ub or anti-HA antibody.

Immunofluorescence Staining. MCF-7 cells were cotransfected with Myc-NCL and Flag-VHL plasmids. After 24 h, cells were treated with 25 nM ZL216 for 5 h, fixed with 4% paraformaldehyde for 15 min and washed three times with DPBS. Cells were permeabilized with 0.2% Triton X-100 for 10 min before blocking in 5% BSA for 1 h and incubation with the primary antibodies at 4 °C overnight. Subsequently, cells were washed and labeled using secondary antibodies conjugated to Alexa Fluor 488 or Alexa Fluor 633 (Thermo Fisher) at room temperature for 1 h. Finally, a confocal microscope (Zeiss LSM510) was used to acquire fluorescent images.

Cell migration assay. MCF-7 cells were seeded in a 12-well plate to grow until creating 95%–100% confluent monolayers. The monolayers were scratched with a sterile pipette tip and washed with serum-free medium. The remaining

cells were treated with 25 nM ZL216, AS1411 or Control in serum-free medium. To measure cell mobility, we obtained images from the same wounded fields at 0, 24, 48 h under BioTek Imaging (USA). The wound healing area (area not covered by cells) was calculated using ImageJ software (NIH, Bethesda, MD, USA).

MCF-10A cells were plated in in a 12-well-plate to grow until creating 95%–100% confluent monolayers. Cells were incubated with mitomycin C (10 μg/ml) for 2 h to block proliferation, followed by the addition of 50 nM ZL216, AS1411 or Control. Cell migration was determined by measuring cell confluency within the wound region over 24 h, using the BioTek instrument, and analyzed with ImageJ software (NIH, Bethesda, MD, USA).

12 well-transwell chambers (Transwell, Corning Costar) were used to perform transwell migration assays. Briefly, 1×10^4 cells were plated in the upper transwell chamber and incubated with 25 nM/50 nM ZL216, AS1411 or Control in serum-free medium. Then, 0.5 mL complete medium was added in the lower chamber as chemoattractant. After 24 h of incubation, migrated cells on the membrane of the chambers were fixed with 4% paraformaldehyde at room temperature. After 15 min, staining with 0.1% crystal violet was performed, followed by destaining with PBS solution. The number of migrating cells was counted under a microscope in five predetermined fields.

In vivo assay. Five-week-old female athymic BALB/c (BALB/c-nude) mice were used for *in vivo* fluorescence imaging and protein degradation assays. Nude mice were subcutaneously transplanted with 8×10^7 MCF-7 cells or BT474 cells. 100 μL DPBS containing 50 μM Cy5-labeled ZL216, AS1411 or control were injected intravenously through the tail vein. The fluorescence images of live mice were collected using the IVIS Lumina II (Caliper LifeScience, USA). For the *in vivo* degradation experiment, the dissected tumor tissues were determined by Western blot assays as described above.

Acknowledgement

This work was supported by grants from the National Natural Science Foundation of China (21890744 and 81672760), the Hunan Provincial Key Research and Development Plan (2018SK2128) and the Changsha Science and Technology Project (kq2001012).

References

1. Posternak, G., et al., Functional characterization of a PROTAC directed against BRAF mutant V600E. Nat Chem Biol, 2020. 16(11): p. 1170-1178.
2. Raina, K., et al., PROTAC-induced BET protein degradation as a therapy for castration-resistant prostate cancer. Proc Natl Acad Sci U S A, 2016. 113(26): p. 7124-9.
3. Khan, S., et al., A selective BCL-XL PROTAC degrader achieves safe

and potent antitumor activity. Nat Med, 2019. 25(12): p. 1938-1947.

4. Hu, J., et al., Discovery of ERD-308 as a Highly Potent Proteolysis Targeting Chimera (PROTAC) Degrader of Estrogen Receptor (ER). J Med Chem, 2019. 62(3): p. 1420-1442.

5. Mullard, A., Targeted protein degraders crowd into the clinic. Nat Rev Drug Discov, 2021. 20(4): p. 247-250.

6. Ye, M., et al., Generating aptamers by cell-SELEX for applications in molecular medicine. Int J Mol Sci, 2012. 13(3): p. 3341-53.

7. Jiang, F., et al., Progress and Challenges in Developing Aptamer-Functionalized Targeted Drug Delivery Systems. Int J Mol Sci, 2015. 16(10): p. 23784-822.

8. Wu, X., et al., Elucidation and Structural Modeling of CD71 as a Molecular Target for Cell-Specific Aptamer Binding. J Am Chem Soc, 2019. 141(27): p. 10760-10769.

9. Romano, S., et al., Nucleolin-based targeting strategies for cancer therapy: from targeted drug delivery to cytotoxic ligands. Drug Discov Today, 2019. 24(10): p. 1985-2001.

10. Reyes-Reyes, E.M., Y. Teng, and P.J. Bates, A new paradigm for aptamer therapeutic AS1411 action: uptake by macropinocytosis and its stimulation by a nucleolin-dependent mechanism. Cancer Res, 2010. 70(21): p. 8617-29.

11. Soundararajan, S., et al., The nucleolin targeting aptamer AS1411

destabilizes Bcl-2 messenger RNA in human breast cancer cells. Cancer Res, 2008. 68(7): p. 2358-65.

12. Cheng, Y., et al., AS1411-Induced Growth Inhibition of Glioma Cells by Up-Regulation of p53 and Down-Regulation of Bcl-2 and Akt1 via Nucleolin. PLoS One, 2016. 11(12): p. e0167094.

13. Rosenberg, J.E., et al., A phase II trial of AS1411 (a novel nucleolin-targeted DNA aptamer) in metastatic renal cell carcinoma. Invest New Drugs, 2014. 32(1): p. 178-87.

14. Soundararajan, S., et al., Plasma membrane nucleolin is a receptor for the anticancer aptamer AS1411 in MV4-11 leukemia cells. Mol Pharmacol, 2009. 76(5): p. 984-91.

15. Wang, J., et al., Synergistic effect of farnesyl transferase inhibitor lonafarnib combined with chemotherapeutic agents against the growth of hepatocellular carcinoma cells. Oncotarget, 2017. 8(62): p. 105047-105060.

16. Holohan, C., et al., Cancer drug resistance: an evolving paradigm. Nat Rev Cancer, 2013. 13(10): p. 714-26.

17. Wu, Q., et al., Multi-drug resistance in cancer chemotherapeutics: mechanisms and lab approaches. Cancer Lett, 2014. 347(2): p. 159-66.

18. Ma, X., et al., NOD2 inhibits tumorigenesis and increases chemosensitivity of hepatocellular carcinoma by targeting AMPK pathway. Cell Death Dis, 2020. 11(3): p. 174.

19. Sakamoto, K.M., et al., Protacs: chimeric molecules that target proteins to the Skp1-Cullin-F box complex for ubiquitination and degradation. Proc Natl Acad Sci U S A, 2001. 98(15): p. 8554-9.

20. Schneekloth, J.S., Jr., et al., Chemical genetic control of protein levels: selective in vivo targeted degradation. J Am Chem Soc, 2004. 126(12): p. 3748-54.

21. Pettersson, M. and C.M. Crews, PROteolysis TArgeting Chimeras (PROTACs) - Past, present and future. Drug Discov Today Technol, 2019. 31: p. 15-27.

22. Schneekloth, A.R., et al., Targeted intracellular protein degradation induced by a small molecule: En route to chemical proteomics. Bioorg Med Chem Lett, 2008. 18(22): p. 5904-8.

23. Fischer, E.S., et al., Structure of the DDB1-CRBN E3 ubiquitin ligase in complex with thalidomide. Nature, 2014. 512(7512): p. 49-53.

24. Galdeano, C., et al., Structure-guided design and optimization of small molecules targeting the protein-protein interaction between the von Hippel-Lindau (VHL) E3 ubiquitin ligase and the hypoxia inducible factor (HIF) alpha subunit with in vitro nanomolar affinities. J Med Chem, 2014. 57(20): p. 8657-63.

25. Buel, G.R., et al., Structure of E3 ligase E6AP with a proteasome-binding site provided by substrate receptor hRpn10. Nat Commun, 2020. 11(1): p. 1291.

26. Lai, A.C., et al., Modular PROTAC Design for the Degradation of Oncogenic BCR-ABL. Angew Chem Int Ed Engl, 2016. 55(2): p. 807-10.

27. Li, F., et al., A water-soluble nucleolin aptamer-paclitaxel conjugate for tumor-specific targeting in ovarian cancer. Nat Commun, 2017. 8(1): p. 1390.

28. Bates, P.J., et al., Discovery and development of the G-rich oligonucleotide AS1411 as a novel treatment for cancer. Exp Mol Pathol, 2009. 86(3): p. 151-64.

29. Xu, X., et al., Inhibition of DNA replication and induction of S phase cell cycle arrest by G-rich oligonucleotides. J Biol Chem, 2001. 276(46): p. 43221-30.

30. Zou, Y., D. Ma, and Y. Wang, The PROTAC technology in drug development. Cell Biochem Funct, 2019. 37(1): p. 21-30.

31. Schapira, M., et al., Targeted protein degradation: expanding the toolbox. Nat Rev Drug Discov, 2019. 18(12): p. 949-963.

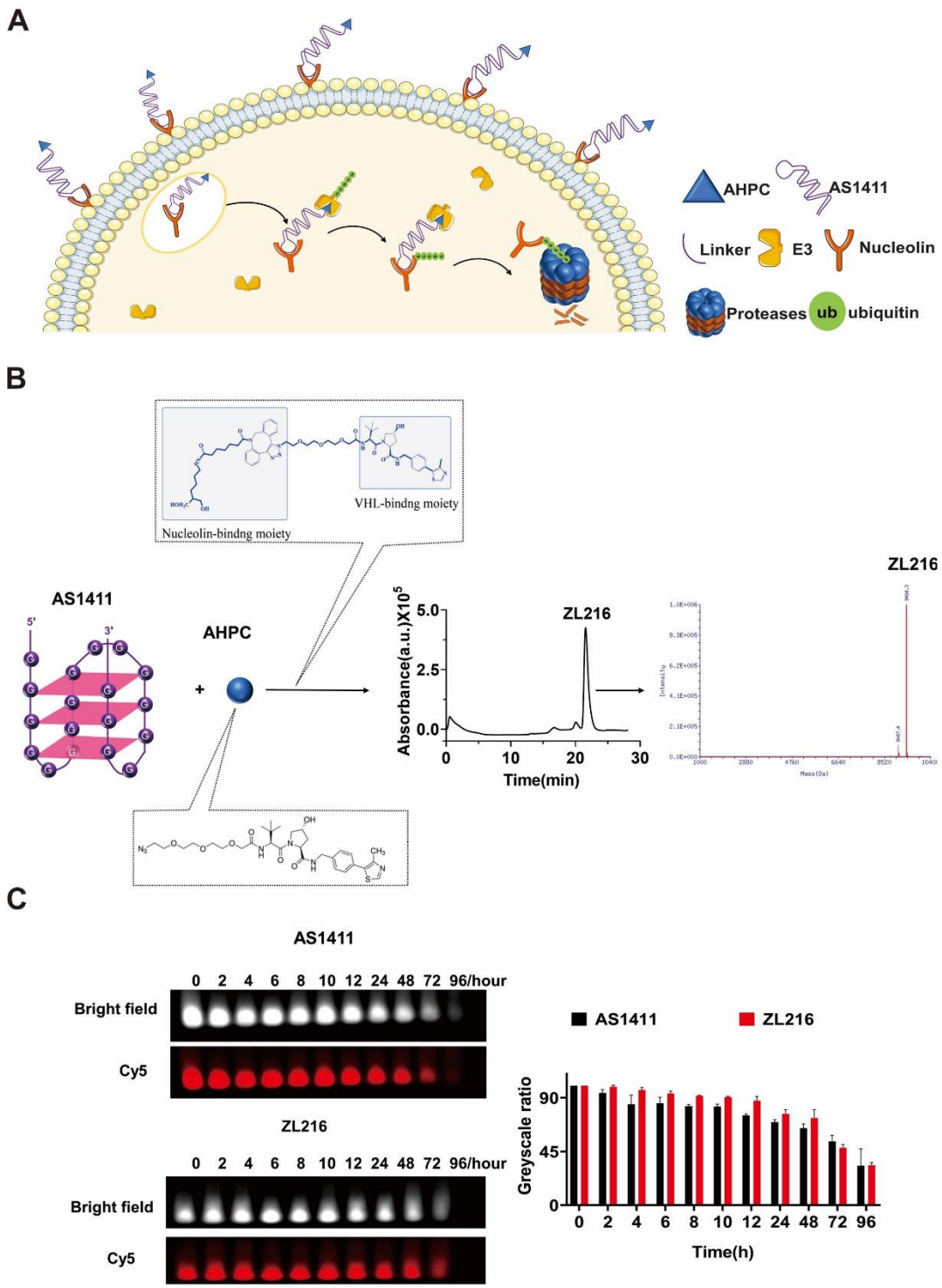

Figure 1. Development of aptamer-based PROTAC ZL216. (A) Presumed mode of action of ZL216 on degradation of nucleolin in cancer cell. (B) Synthetic roadmap and LC-MS analysis of ZL216. (C) Agarose gel electrophoresis and quantitative analysis of AS1411 and ZL216 in human serum.

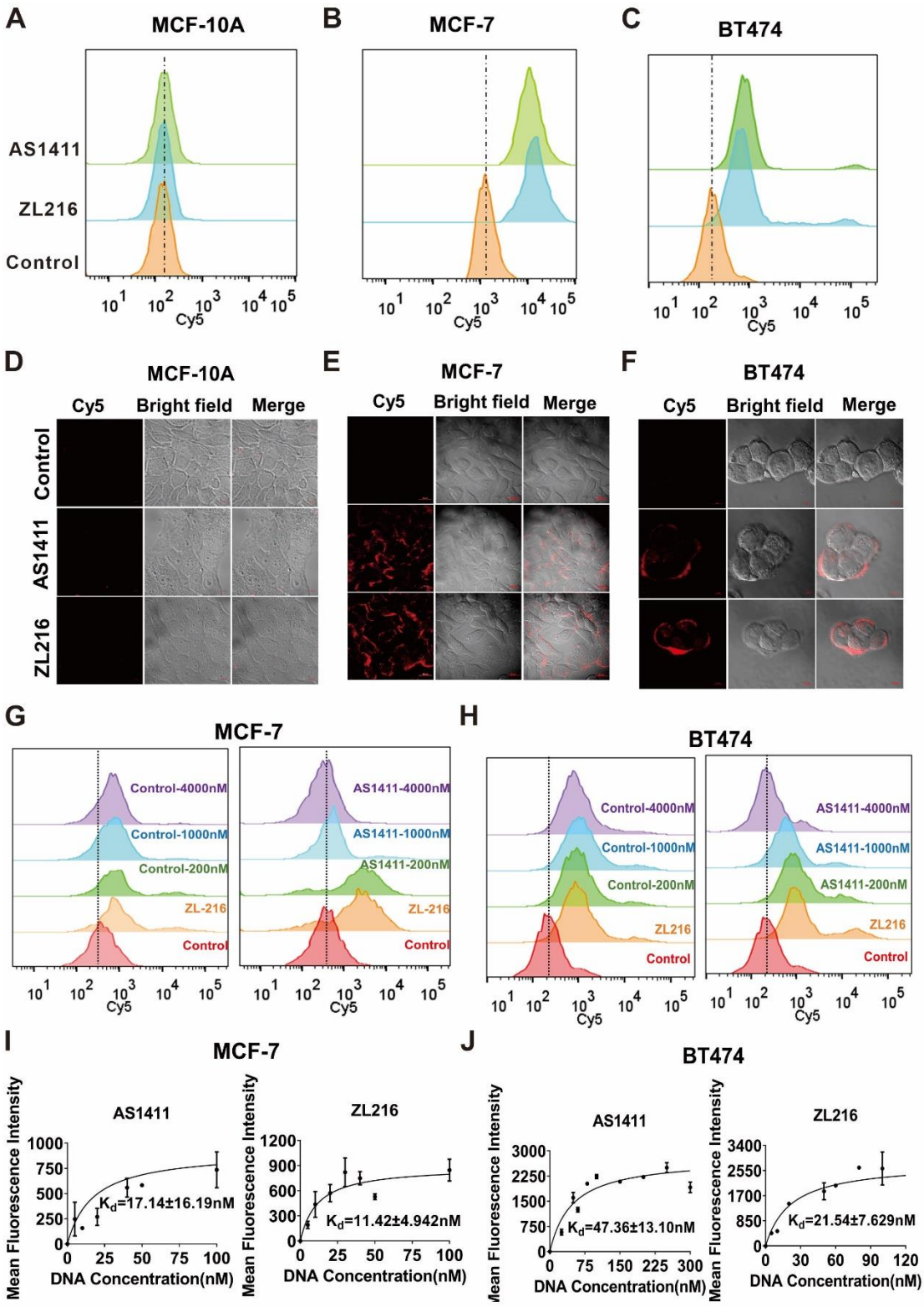

Figure 2. ZL216 selectively binds to breast cancer cells. (A-C) The binding of ZL216 and AS1411 to MCF-10A (A), MCF-7 (B) and BT474 (C) cells was analyzed by flow cytometry. (D-F) MCF-10A (D), MCF-7 (E) and BT474 (F) cells

were incubated with Cy5-labeled ZL216 and AS1411. Fluorescence, bright-field, and merged confocal images were shown. (G-H) MCF-7 (G) and BT474 (H) cells were incubated with the indicated concentration of AS1411, followed by treatment with Cy5-ZL216. Competition binding was analyzed by flow cytometry. (I-J) The dissociation constant of AS1411 and ZL216 for MCF-7 (I) and BT474 (J) cells was determined by flow cytometry.

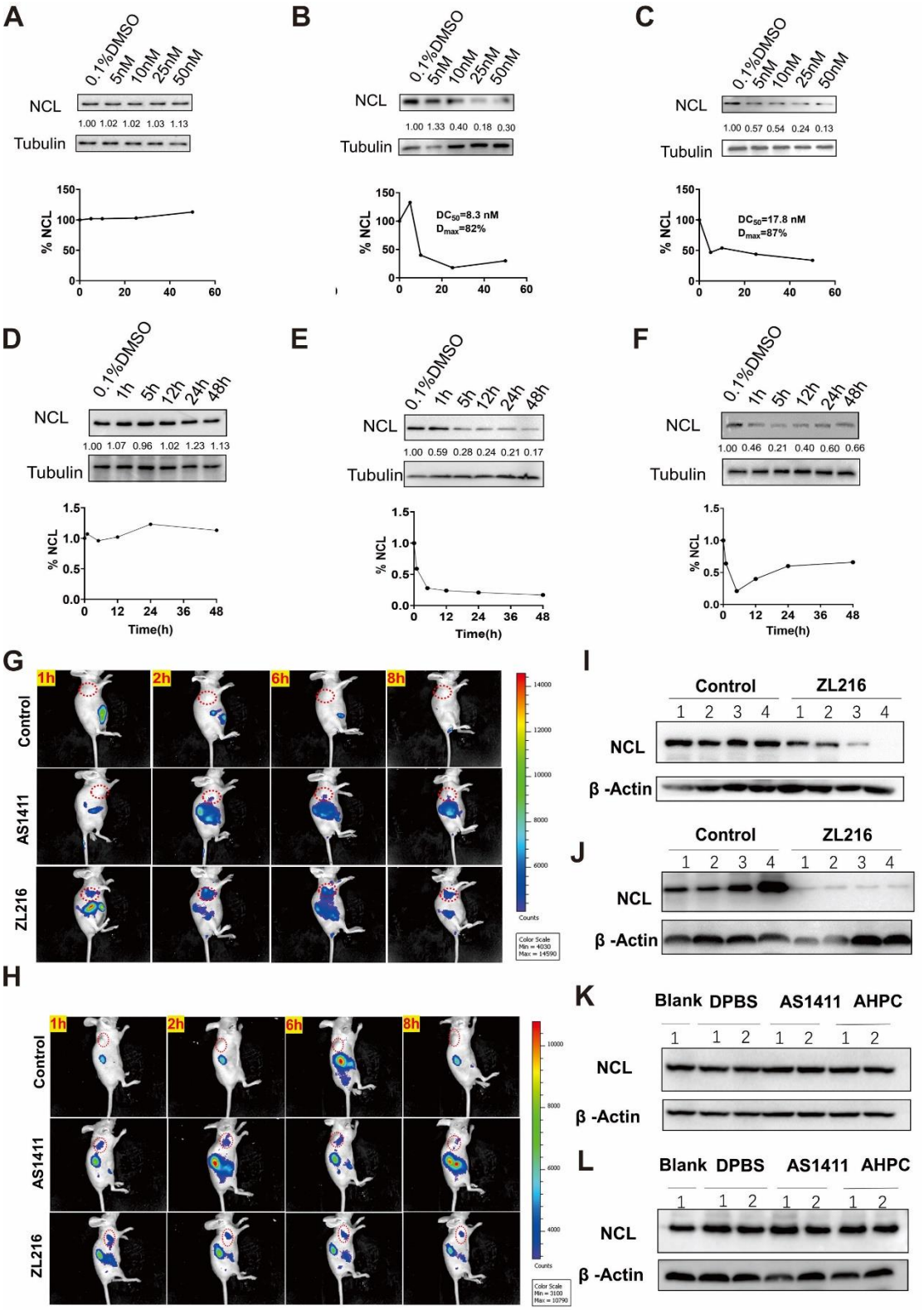

Figure 3. ZL216 downregulates the nucleolin of breast cancer cells *in vitro* and *in vivo*. (A-C) MCF-10A (A), MCF-7 (B) and BT474 (C) cells were treated with the indicated concentration of ZL216. Total protein was extracted and subjected

to Western blotting using the indicated antibodies. (D-F) ZL216-treated cells at the concentration of 50 nM (MCF-10A) (D), 25 nM (MCF-7) (E) and 50 nM (BT474) (F). Total protein was extracted at the indicated time points and subjected to Western blotting using the indicated antibodies. (G-H) MCF-7 cells (G) and BT474 cells (H) were injected subcutaneously into nude mice. When tumors grew to desired size, Cy5-labeled AS1411, ZL216 or Control was injected intravenously into nude mice. The fluorescence images *in vivo* were shown at the indicated time points. (I-J) MCF-7 (I) and BT474 (J) tumor-bearing mice were injected intravenously with ZL216 or control. Total protein was extracted from tumor tissues and subjected to Western blotting using the indicated antibodies. (K-L) MCF-7 (K) and BT474 (L) tumor-bearing mice were injected intravenously with AS1411, AHPC or DPBS. Total protein was extracted from tumor tissues and subjected to Western blotting using the indicated antibodies.

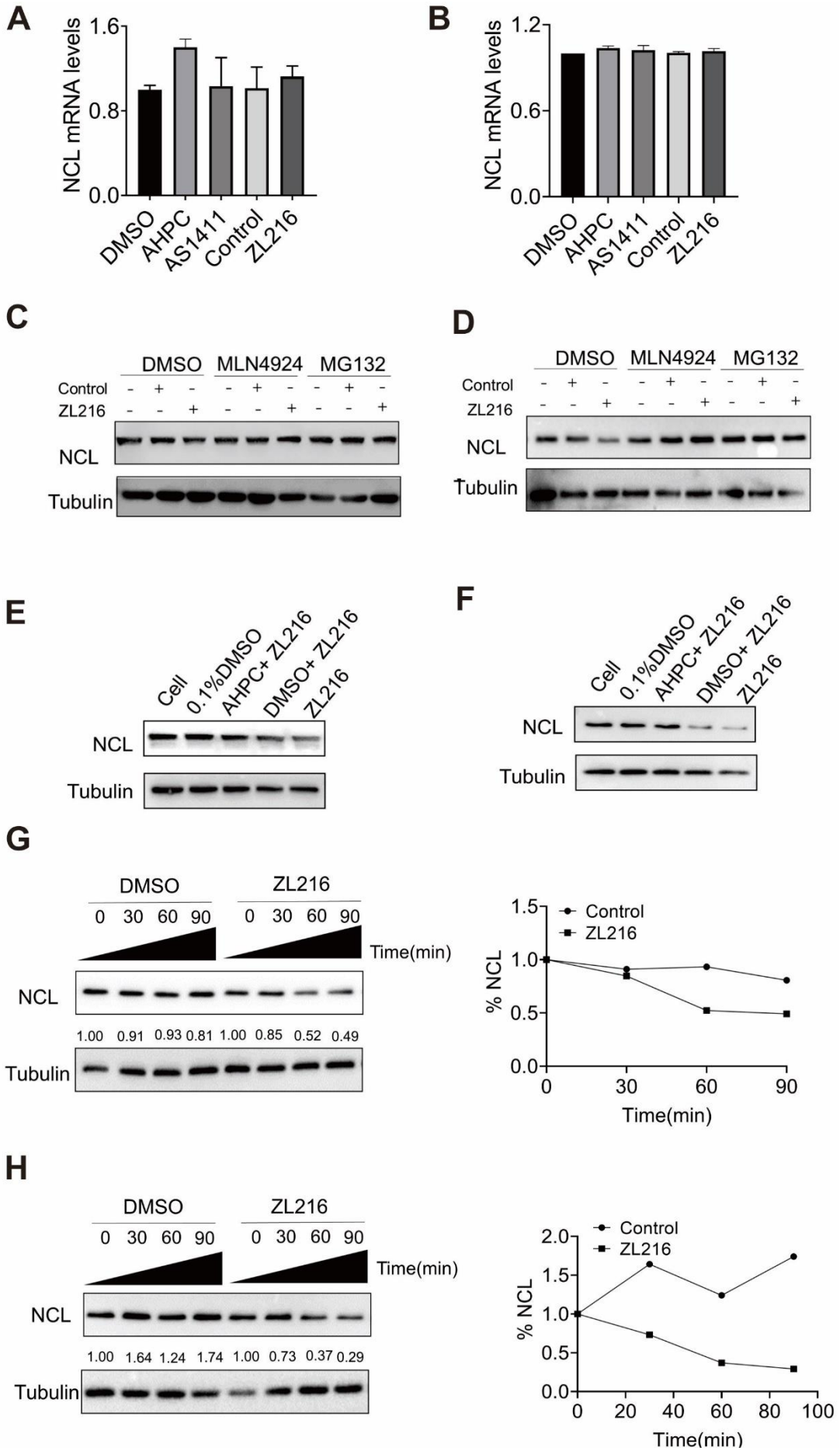
A
NCL mRNA levels
1.6
0.8
0.0
DMSO
AHPC
AS1411
Control
ZL216
B
NCL mRNA levels
1.2
0.6
0.0
DMSO
AHPC
AS1411
Control
ZL216
C
DMSO
MLN4924
MG132
Control
ZL216
NCL
Tubulin
D
DMSO
MLN4924
MG132
Control
ZL216
NCL
Tubulin
E
Cell
0.1%DMSO
AHPC+ ZL216
DMSO+ ZL216
ZL216
NCL
Tubulin
F
Cell
0.1%DMSO
AHPC+ ZL216
DMSO+ ZL216
ZL216
NCL
Tubulin
G
DMSO
ZL216
0 30 60 90
0 30 60 90
Time(min)
NCL
1.00 0.91 0.93 0.81 1.00 0.85 0.52 0.49
Tubulin
Control
ZL216
% NCL
1.5
1.0
0.5
0.0
0 30 60 90
Time(min)
H
DMSO
ZL216
0 30 60 90
0 30 60 90
Time(min)
NCL
1.00 1.64 1.24 1.74 1.00 0.73 0.37 0.29
Tubulin
Control
ZL216
% NCL
2.0
1.5
1.0
0.5
0.0
0 20 40 60 80 100
Time(min)

Figure 4. ZL216 redirects E3 ubiquitin ligase VHL to degrade NCL proteins via the proteasomal pathway. (A-B) Total RNA from MCF-7 (A) or BT474 (B) cells treated with control, AHPC, AS1411 or ZL216 was isolated and subjected to qRT-PCR. The error bars represent the SD of triplicate measurements. (C-D) MCF-7 (C) or BT474 (D) cells were pretreated with DMSO, MLN4924 (5 μM) or MG132 (20 μM), followed by ZL216 treatment for 5 h. The indicated proteins were analyzed by Western blotting. (E-F) MCF-7 (E) or BT474 (F) cells were incubated with AHPC (1μM), followed by ZL216 treatment for 5 h. The indicated proteins were analyzed by Western blotting. (G-H) MCF-7 (G) or BT474 (H) cells were incubated with 100 μg·mL−1 CHX for 1 h, followed by ZL216 treatment for 5 h. Total proteins were extracted at the indicated time points and subjected to Western blotting using the indicated antibodies.

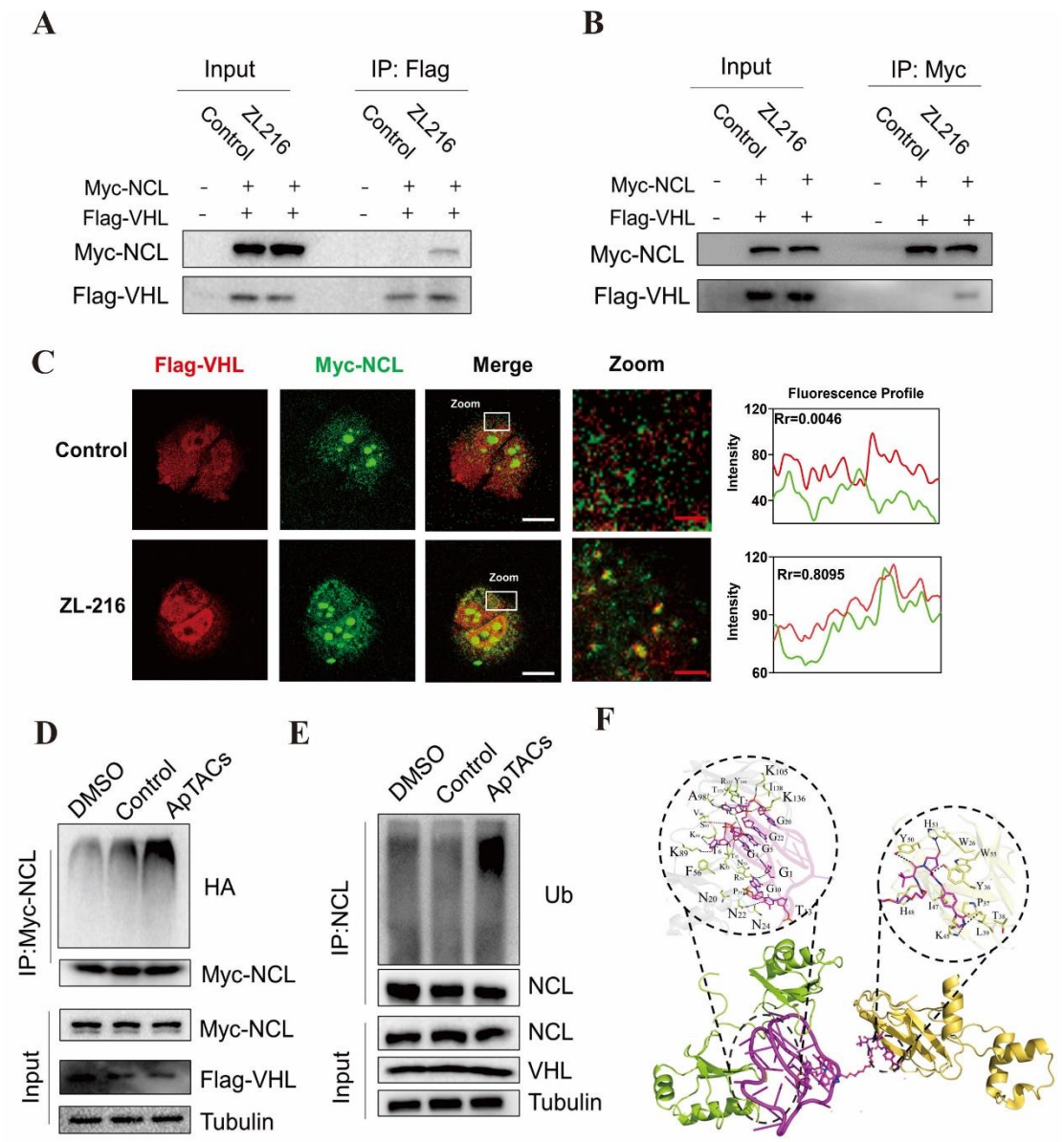

Figure 5. ZL216 mediates nucleolin-ZL216-VHL ternary complex formation. (A-B) MCF-7 cells transfected with plasmids expressing Flag-VHL and Myc-NCL were treated by ZL216 or control treatment for 5 h. Total cell lysates were subjected to immunoprecipitation with anti-Flag (A) or anti-Myc (B) antibody. The immunoprecipitates were then analyzed by Western blotting using the indicated antibodies. (C) MCF-7 cells transfected with the indicated plasmids were treated with ZL216 or control for 5 h. The subcellular localization of VHL and nucleolin was visualized using immunofluorescence with the indicated

antibodies. (D) MCF-7 cells transfected with plasmids expressing Myc-NCL and HA-Ub were incubated with MG132 (20μM) for 1 h, followed by treatment with DMSO, control or ZL216 for 5 h. Mycl-NCL was immunoprecipitated with anti-Myc antibody, and the immunoprecipitates were probed with the indicated antibodies. (E) MCF7 cells were incubated with MG132 (20μM) for 1 h, followed by treatment with DMSO, control or ZL216 for 5 h. Nucleolin was immunoprecipitated with an anti-nucleolin antibody, and the immunoprecipitates were probed with the indicated antibodies. (F) Predicting optimal conformation of NCL: ZL-216: VHL ternary complex. Light green dashes indicate the NCL structure, and blue cartoons are VHL E3 ligase. Magenta dashes represent ZL-216.

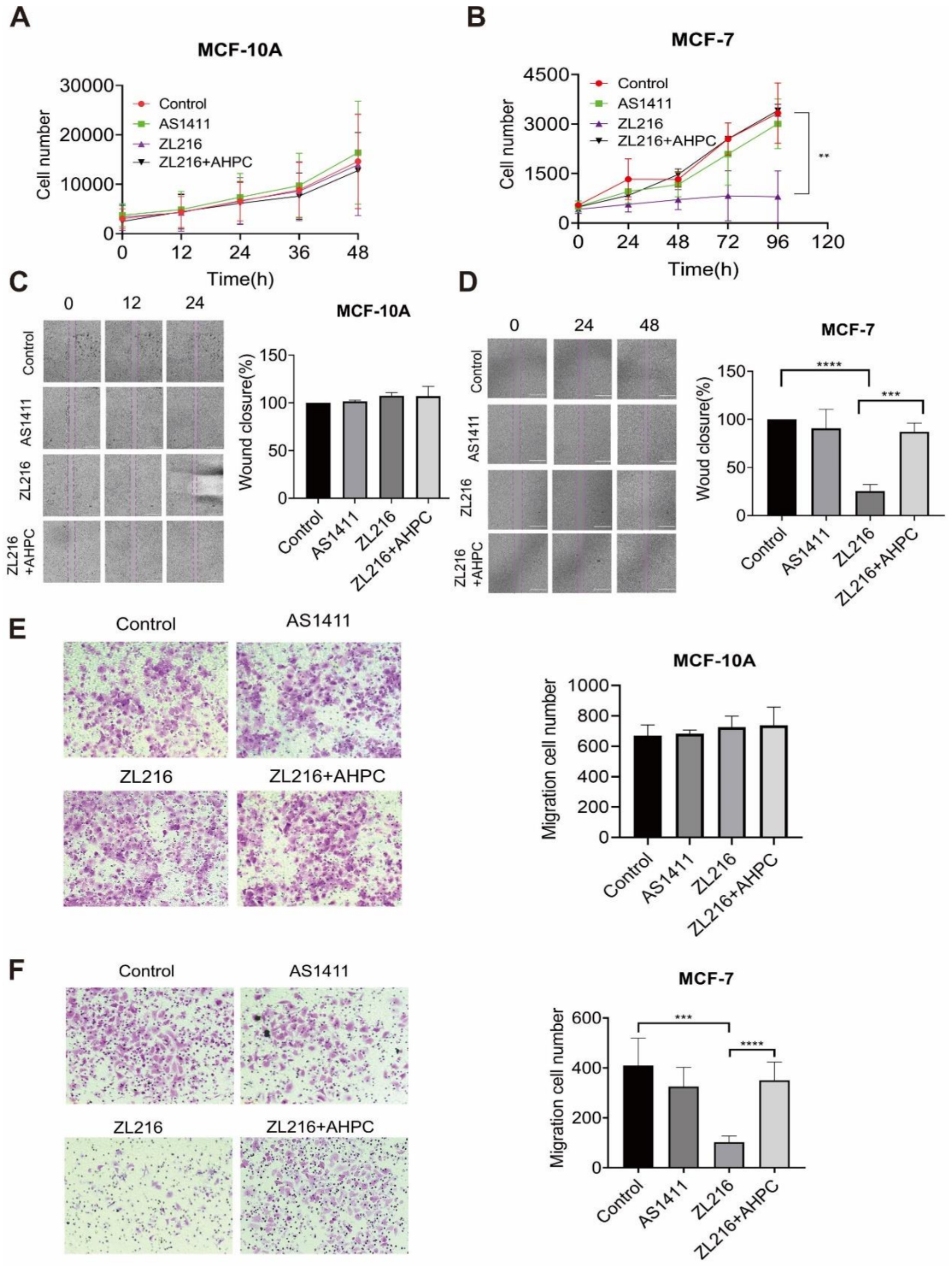

Figure 6. ZL216 inhibits the proliferation and migration of breast cancer cells. (A-B) MCF-10A (A) or MCF-7 (B) cells were incubated, or not, with 1μM AHPC for 1h, followed by the treatment with ZL216, AS1411 or control. Cell number was calculated at the indicated time points. (C-D) MCF-10A (C) or MCF-7 (D)

cells were incubated, or not, with 1μM AHPC for 1h, followed by treatment with ZL216, AS1411 or control. Scratches were made and wound healing was observed in the indicated time points. (E-F) MCF-10A (E) or MCF-7 (F) cells were incubated, or not, with 1μM AHPC for 1h, followed by treatment with ZL216, AS1411 or control. The cells that had migrated though the pores were stained and quantified by counting five independent visual fields. (* *P<0.05, * * *P<0.001, * * * *P<0.0001).